Arch. Metall. Mater. **65** (2020), 1, 423-431

DOI: 10.24425/amm.2020.131745

W. PRESZ[1*]

INFLUENCE OF EXPERIMENTAL SETUP PARAMETERS ON ULTRASONIC ASSISTED MICRO-UPSETTING

The progressive development of miniature systems increases the demand for miniature parts. Reducing the size of manufactured components on one hand is a serious challenge for traditional technologies, but on the other hand, mainly by removing the energy barrier opens the possibility of using other unconventional techniques. A good example is the ultrasonic excitation of the punch during the micro-upsetting process. The anti-barreling phenomenon and dependent on the amplitude of vibrations, intensive deformation of the surface layers in contact with the tools at both ends of the sample was noted. Based on the measured strains and stresses, an increase in temperature in the extreme layers to approx. 200°C was suggested. By adopting a simplified dynamic model of the test stand, the possibility of detaching the surface of the punch from the surface of the sample was demonstrated.

Keywords: Microforming, Ultrasonic, Dynamic effect, Elastic deflection

1. Introduction

The progressive development of miniature electro-mechanical systems, micro-robots, micro-sensors, or in general – progressive miniaturization of mechanisms, increases the demand for miniature parts [1,2]. This is the driving force and challenge for miniaturization of virtually all material technologies. Among them, the metal forming technology plays a significant role. Its miniaturization is associated with serious difficulties. The occurrence of the limit size of the manufactured parts has been observed, below which changes the nature of the physical interactions that take place. The technologies developed so far require modification or even a new approach. Such a limiting dimension is 1 mm understood as at least two dimensions of the classified object. As a result, a new branch of metal forming was created that deals with the production of objects that meet the above criterion [3]. It is a microforming [4]. Deviations from the developed technology rules for years associated with miniaturization are called "scale effects". They concern, in principle, all elements of the technological process. Surface layer and contact phenomena [5], affecting the friction [6,7], lubrication [8] and galling [9], increasing the role of preparation methods for micro-billets surfaces [10,11]. They also refer to the billet design material distribution [12] internal structure [13,14], which affects the quality of the surface and cracking mechanisms [15]. Scale effect concern even the construction of machines [16], tooling [17,18] and tools [19,20] and design of the technological process plan [21,22]. Reducing the size of manufactured parts on the one hand is a serious challenge for traditional technologies, but on the other hand, mainly by removing the energy barrier opens the possibility of using other unconventional techniques. You can mention here: electric power assistance, magnetic wave, laser treatment and mechanical vibrations of various frequencies. In the last of these methods, ultrasonic vibrations are particularly in the sphere of greatest interest. The history of trials to apply ultrasonic vibrations in forming process dates back to the 50s of the last century. Gale and Nevill (1957) [23] applied ultrasounds in a test of drawing low-carbon steel wire. Standing longitudinal waves were generated. Based on the research, they suggested that the observed decrease in yield stress is independent of the vibration frequency in the range of 15-80 kHz. Blaha and Langenecker (1959) [24] after similar experiments also stated that the "softening" of the material is independent of the frequency of vibrations when the frequency is from 15 kHz to 106 kHz. From that time more and more studies showed the impact of ultrasonic assistance on process and product parameters especially during microforming processes. Ultrasonic-vibration can reduce the ECAP [25] and micro-extrusions forces when friction is almost eliminated [26]. On another hand can increase the temperatures of a material at the same time. Increasing temperature by ultrasonic-vibration may reduce the flow stress, but may increase the interfacial friction in hot and cold micro-upsetting

[1] WARSAW UNIVERSITY OF TECHNOLOGY, INSTITUTE OF MANUFACTURING TECHNOLOGIES, 85 NARBUTTA STR., 02-524, WARSZAWA, POLAND

* Corresponding author: w.presz@wip.pw.edu.pl

[27]. However, in some cases, the maximum forming force can exceed the static forming force [28]. The use of ultrasonic vibrations in relation to microformed objects can also cause specific macroscopic consequences in terms of cracking. Investigating samples made of hardened aluminium, Presz and Cacko (2017) [29] observed the formation of many parallel fracture surfaces being "on line" welded during micro-upsetting process. In studies on the influence of ultrasonic vibrations on the course of the microforming process, the often used is micro-upsetting under dry friction conditions [30,31] due to geometric simplicity and relative ease for modelling. In some conditions of upsetting with the use of ultrasonic vibrations, the formation of a specific shape of the lateral surface of the sample is reported [32-34]. The phenomenon leading to it was taken to call "anti-barrelling". The name is a reference to the phenomenon called "barrelling" [35], which concerns the formation of the convex side surface of the upset cylinder. It is created as a result of friction forces occurring on the contact surfaces with tools. Anti-barrelling is the formation of a concave lateral surface. This effect is not being observed in any upsetting conditions involving ultrasonic vibrations [36, 37]. The causes and consequences of this phenomenon are not fully explained and are currently under investigation. One of the hypotheses is the temporary detachment of the surface of the punch from the surface of the sample [33,38]. The work presented below refers to this phenomenon.

2. Experimental setup

Experimental setup, Fig. 1, consists of a testing machine – 1 and a die set placed on it – 2, on whose lower plate a micro-die set – 3 is mounted and an ultrasonic system, Fig. 1c. Ultrasonic head consists of piezoelectric transducer – 4, booster – 5 and sonotrode – 6 with punch – 7. An alternating current oscillating at ultrasonic frequency is applied by a power supply unit to the piezoelectric transducer. Booster and sonotrode work as half-wavelength resonators, vibrating lengthwise with standing waves at its resonant frequency. The frequency used is 20 kHz. It is possible to adjust the amplitude indirectly, that is, by changing the power supplied. Sonotrode acts as a displacement amplifier.

On the basis of the laser displacement transducer, the amplitude of the vibrations on the surface of the booster and the face of the punch was determined by the amplitude dependence on the given power in the range of 20-60%. The results are shown in Table 1.

TABLE 1

The test results of the ultrasonic system

	Amplitude		
Applied power	**On the surface of the booster**	**On the surface of the punch**	**Amplification**
%	**µm**	**µm**	**1**
20	1.8	5.8	3.2
30	2.3	9.9	4.3
40	2.5	16.0	6.3
60	2.7	18.6	6.9

Specimens were blanked from 1 mm thick aluminum sheet metal of type A1 99.5 (ISO), state H12 (R_{02} = 65 MPa).

3. Experiment results

The sample before the upsetting process and the sample after upsetting without and with vibration assistance are shown in Fig. 2a-d. The registered forces of processes are shown in Fig. 3.

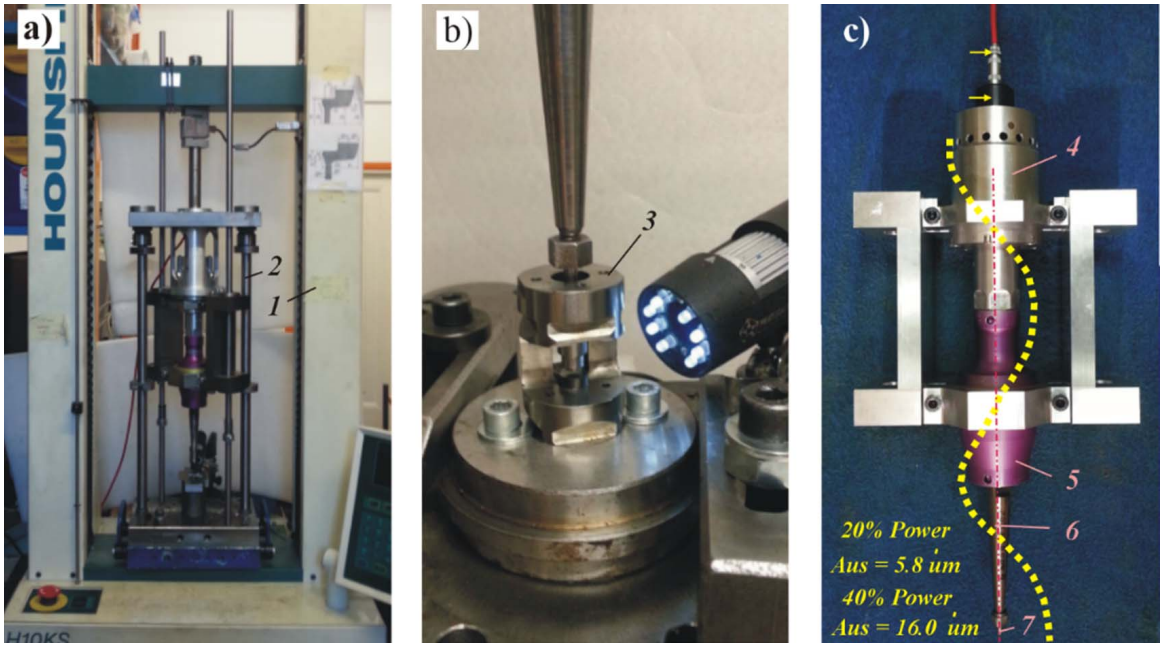

Fig. 1. Experimental stand: 1 – testing machine, 2 – die set, 3 – micro-die set, 4 – ultrasonic transducer, 5 – booster, 6 – sonotrode, 7 – punch, 8: (a) overview, (b) close-up of working area, (c) ultrasonic system – the dotted yellow line expresses local amplitude of the standing wave

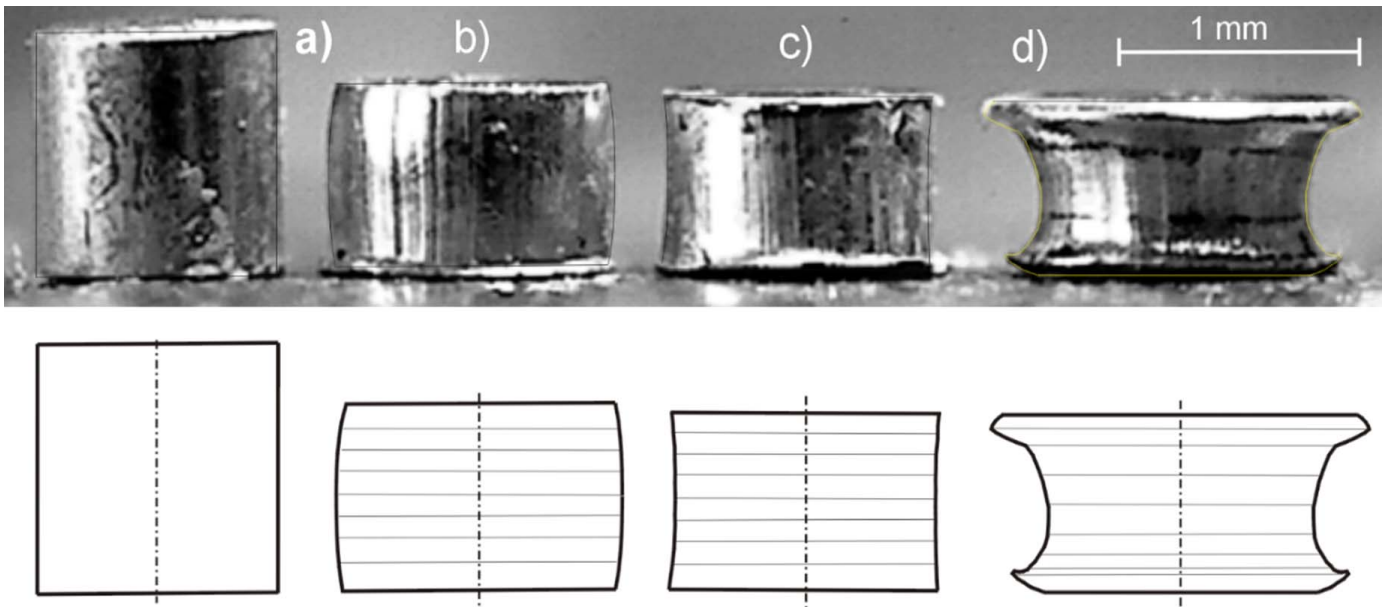

Fig. 2. Samples, their outlines and considered layers: (a) initial shape, (b) after deformation – no vibration – 0% power, (c) after deformation – 20% power, (d) after deformation – 40% power

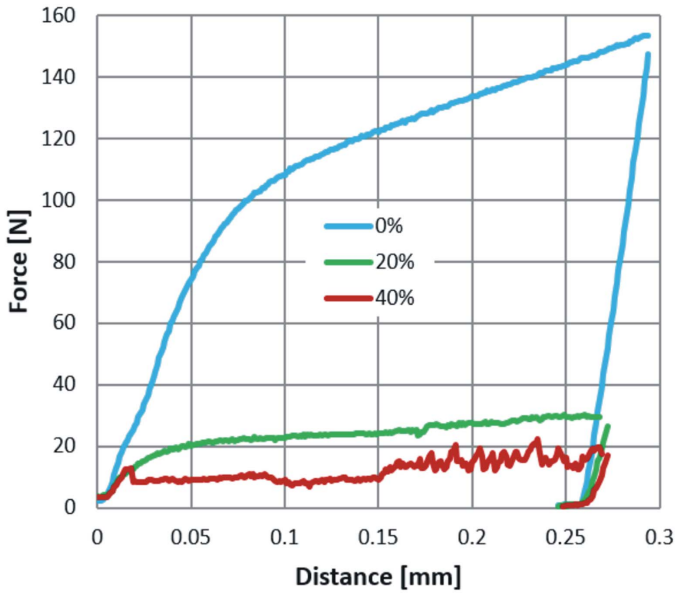

Fig. 3. Registered process forces: no vibration, 20% of power, 40% of power

4. Analysis of results

Using the method presented in [40] strains and stresses were estimated in subsequent sections of the samples using the dimensions shown in Fig. 2a-d. The concept of the method used is explained in Fig. 4a. On the basis of the external outline, the axial component of the strain, Eq. (1), Fig. 4b and the axial component of the stress Eq. (2) are determined, Fig. 4c.

Calculated values of stresses for experiments with vibrations are completely unreliable and result from an unreliable measurement of forces probably due to the dynamic nature of the processes and position of force transducer, see Fig. 6.

$$\varepsilon_{l(0,20,40)i} = \left| \ln \frac{A_{(0,20,40)i}}{A_b} \right|, \quad i = 0,1,\ldots,n \tag{1}$$

$$\sigma_{l(0,20,40)i} = \frac{F_{(0,20,40)}}{A_{(0,20,40)i}}, \quad i = 0,1,\ldots,n \tag{2}$$

where: $A_{(0,20,40)}$ – cross-sections of deformed specimens, the meaning of indexes: no vibration (0), 20% power (20) and 40% power (40), A_b – cross-section of billet

The process force in each layer can be represented as Eq. (4).

$$\wedge_1 F_{(20,40)i} = F_{(20,40)} =$$
$$= \sigma_{l(20,40)i} \cdot k_{\sigma(20,40)i} \cdot A_{(20,40)i} \cdot k_{A(20,40)i} \tag{3}$$

$$k_{\sigma(20,40)i} \cdot k_{A(20,40)i} = 1, \quad i = 0,1,\ldots,n \tag{4}$$

$$k_{\sigma(20,40)i} = \frac{\sigma_{(20,40)i}}{\sigma_{(0)i}}, \quad i = 0,1,\ldots,n \tag{5}$$

$$k_{A(20,40)i} = \frac{A_{(20,40)i}}{A_{(0)i}}, \quad i = 0,1,\ldots,n \tag{6}$$

where: k_σ – stress coefficient, k_A – cross-section coefficient

$$k_T(T) = \frac{Y(T)}{Y(T_{ref})} \tag{7}$$

$$\wedge_{k_{\sigma(20,40)}} \vee_{k_T} \frac{1}{k_T} = k_A \tag{8}$$

where: $Y(T)$ yield stress as a function of temperature, T_{ref} – temperature of 20°C, k_T – yield stress coefficient.

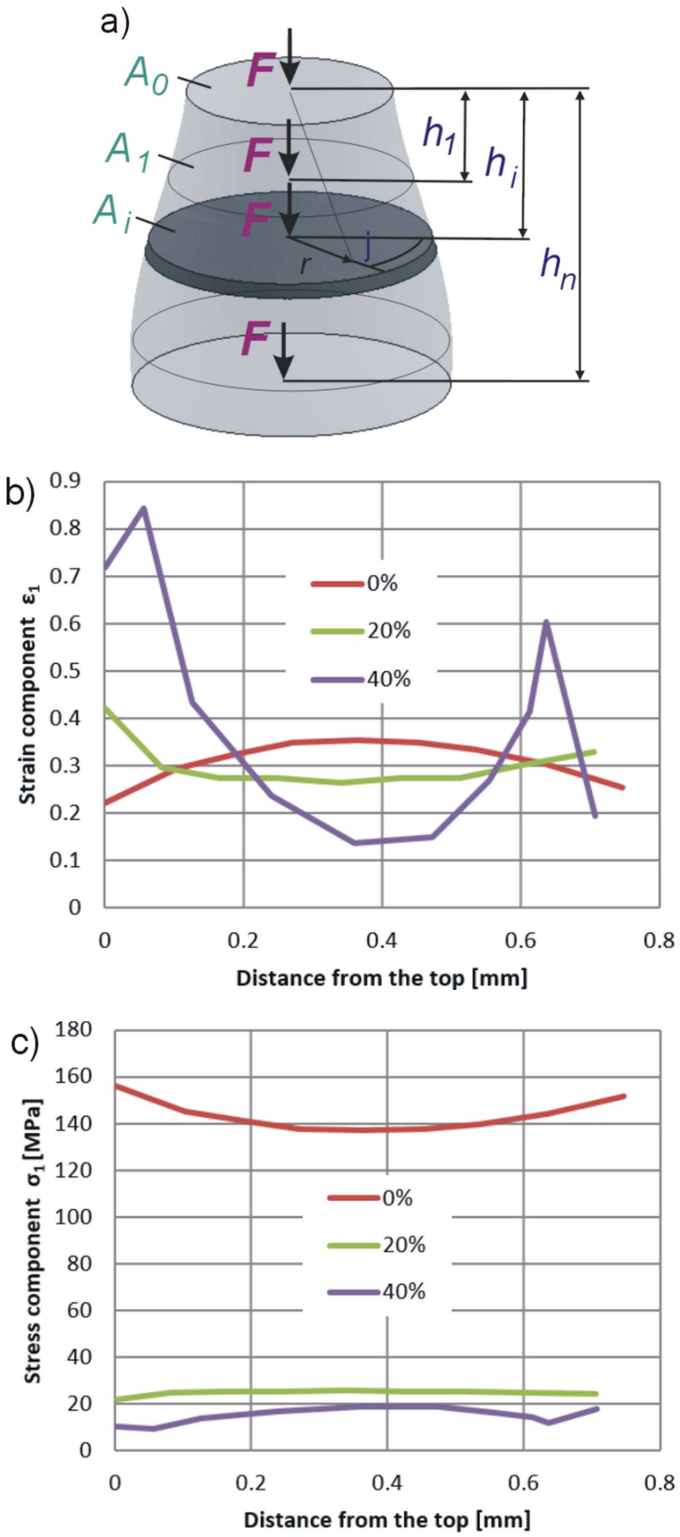

Fig. 4. (a) The concept of analysis [39], (b) axial strain component, (c) axial stress component

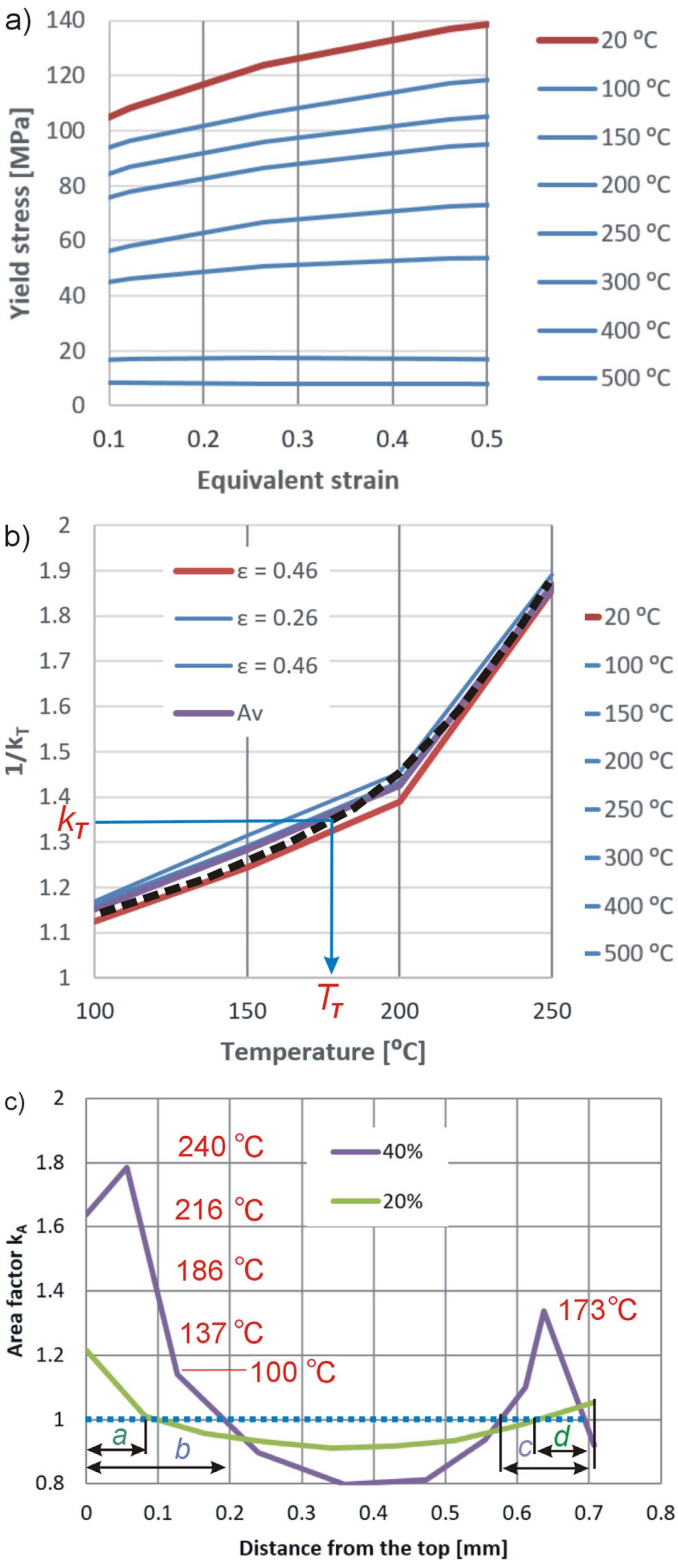

Fig. 5. (a) Stress-Strain curves for billet [39], (b) the inverse of cross-section coefficient, (c) the hypothetical temperature increase

In accordance with Fig. 4a, a hypothetical increase in temperature was determined resulting in a lowering of the yield point and an increase in deformation in the upper and lower layers of the sample. The procedure is as follow. Based on the literature information about the stress-strain curves [40], Fig. 5a, the inverse diameter of the coefficient k_T as a function of temperature, Fig. 5b. along the lines *a*, *b* and *c* was determined.

On the basis of Eq. (8) from the graph Fig. 5b, temperatures corresponding to the values of coefficient k_A are found. These temperatures are shown in the graph of Fig. 5c. It shows the range of areas of temperature increase.

Liu et al. (2013) [37] reached a similar conclusion – regarding temperature rise – explaining this by the temporary loss of the

tool contact with the workpiece. The loss of contact was also suggested by Hu et al. (2017) [38]. In the event of temporary loss of contact, the occurrence of the anti-barreling phenomenon seems to be facilitated by facilitating the radial flow of the material. This situation is also conducive to the increase in temperature, because the heat generated by the rapid plastic deformation at the moment of loss of contact does not flow to the tools.

Do the conditions of the conducted experiments cause temporary loss of contact? This is suggested by the stored process waveforms - which are unbelievable low. To answer the question of whether the "dynamic effect" occurred in performed investigations, and thus whether the punch could detach from the sample surface, the analysis presented below was carried out.

5. Analysis of the experimental setup

The layout of the setup is shown in Fig. 6.

The sample 1 is placed on the face of the fixed lower punch – 2 placed in the Micro-tool set – 3 on the table 4 of the testing machine. The sample is deformed using the upper punch – 5, which is placed at the end of the sonotrode – 6 of the ultrasonic system (7 – booster, 8 – sandwich transducer). The ultrasonic system is mounted in the frame – 9, which through the force transducer – 10 is connected to the ram 11 of the testing machine.

The stand has been simplified to four elements: 1. an equivalent assembly of the machine (elastic – E_e), 2. a vibrator with constant amplitude (no dumping) and frequency (Q-R, quasi rigid), 3. an elastically returning sample (E_1 elastic) and 4. an elastic lower punch (elastic E_2).

Imagining the situation of the extreme position in which the vibrator is elongated A_{us}, the sample is deformed and its elastic return is A_s, the lower punch deflected A_c and the loading system (LS) elastically deformed A_L.

Now the punch moves back by $2A_{us}$ with the acceleration resulting from the frequency of the oscillating system $f = 20$ kHz. Behind the punch, the elastic sample retracts - elastic return with acceleration resulting from its natural frequency f_s and the lower punch – elastic recovery with acceleration resulting from its own frequency.

The load system is also reversed – elastic recovery with acceleration resulting from its characteristics. The springing back of the sample and the lower punch can be determined from the Eq. (9), and the natural frequency from Eq. (10).

$$A = \frac{\sigma_1 \cdot h}{E} \tag{9}$$

$$f = k \cdot \pi \cdot \sqrt{\frac{E}{\gamma \cdot h^2}} \tag{10}$$

where: see Table 2.

The calculated values are shown in Table 2. The amount of axial stress against the unreliability of the registered force is difficult to determine. With excess, it was calculated based on the cross-sectional increment at the middle of height of the deformed sample, defining the axial deformation in this cross-section and substituting it for the stress-strain curve of the deformed material.

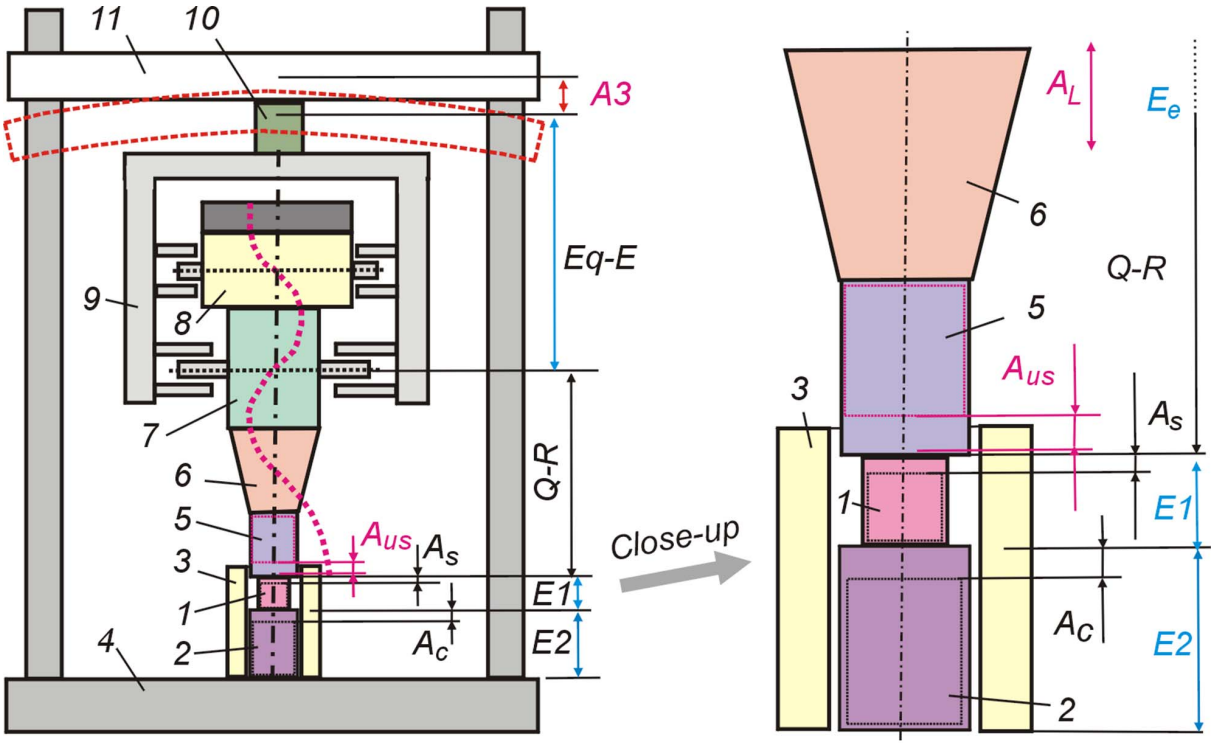

Fig. 6. Scheme of the experimental setup: sample – 1, lower punch – 2, micro-tool set – 3, table of the testing machine – 4, upper punch – 5, sonotrode – 6, booster – 7, sandwich transducer – 8, frame – 9, force transducer – 10, ram of the testing machine – 11. A description of the process parameters shown can be found in the text

TABLE 2

Experimental setup parameters

Part A	**Natural frequency**				
1	Quantity		Specimen	Lower Punch	Dimension
2	Young Mod.	E	7.00E+10	2.00E+11	N/m^2
3	Density	γ	2700	7800	kg/m^3
3	Hight	h	7.00E-04	3.00E-02	m
4	k (Eq. (10))		1	1	1
5	Natural freq.	f	22851724	530269.1	Hz
Part B	**Elastic deflection**				
	Force		Specimen	Lower Punch	
6	143		1.40E-06; 1.4	1.45E-06; 1.45	m; µm
7	110		1.22E-06; 1.2	1.89E-06; 1.89	m; µm
Part C	**Load system**				
8	Stifness	$k_{M/L}$	4304100; 4.3		N/m; N/µm
9	Force		143	110	N
10	Elastic def.	A_L	3.32241E-05; 33.2	2.5557E-05; 25.5	m; µm
11	Period of unload.		0.012	0.012	s

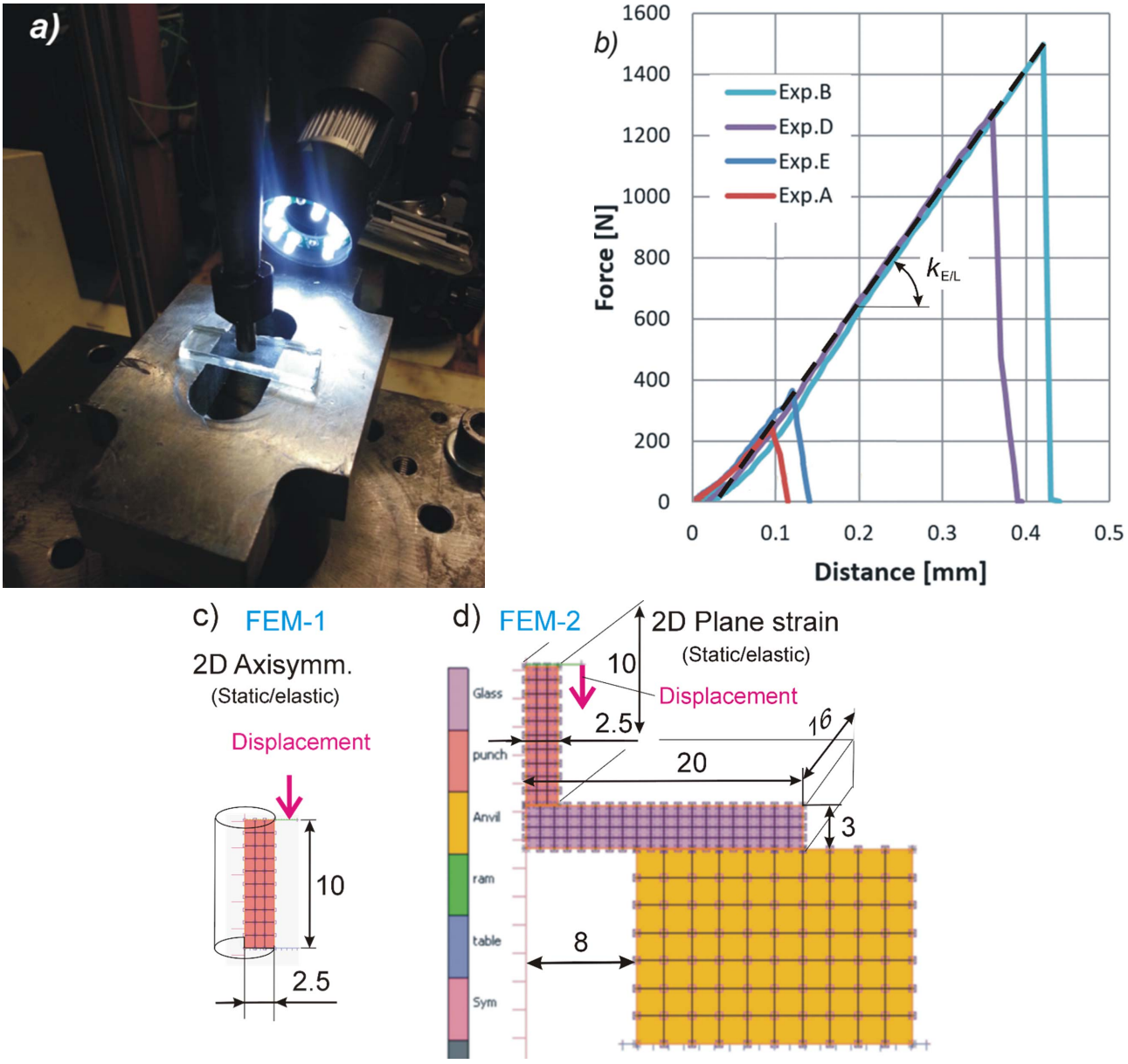

Fig. 7. Glass braking by bending: (a) process overview, (b) registered forces, (c) FEM-1 model, (d) FEM-2 model

6. Analysis of the load system

The analysis is based on the results of two types of experiments and simulations using the FEM. The first of the experiments is the process of simple upsetting cylindrical aluminium samples with the ram velocity of 0.5 mm / min and the unloading speed 0.05 mm / min. The second process is the process of breaking glass samples in the bending condition, shown in Fig. 7a with force registration, Fig. 7b. This bending was simulated statically with the FEM using commercial MS Marc 2017.0.0 software. In the FEM-1 (2D Asymmetrical) analysis, Fig. 7c, stiffness k_A of the punch was determined. In the second analysis, see Fig. 7d, the stiffness k_G of the glass sample in bending condition was determined. Young modules and Poisson's ratios were used for simulations, respectively: for punch 210 GPa and 0.32, and for glass: 72 GPa and 0.3.

Selected results in the form of force records in the displacement function are shown collectively in Fig. 8a. Selected results of force drop after fracture of glass samples as a function of time are shown in Fig. 8b. It points out that the lines converge at one point, which confirms the credibility of data acquisition system. Time shows the inertia of the load system, Fig. 8b and Table 2 – row 11.

Curves, shown in Fig. 8a, were used for the static analyse of the load system: the unloading curve in the upsetting test – *a* and the loading curve in the glass sample breaking test – *b*. Their courses allow to determine the static stiffness of the system. The method of static system analysis is shown in Fig. 9.

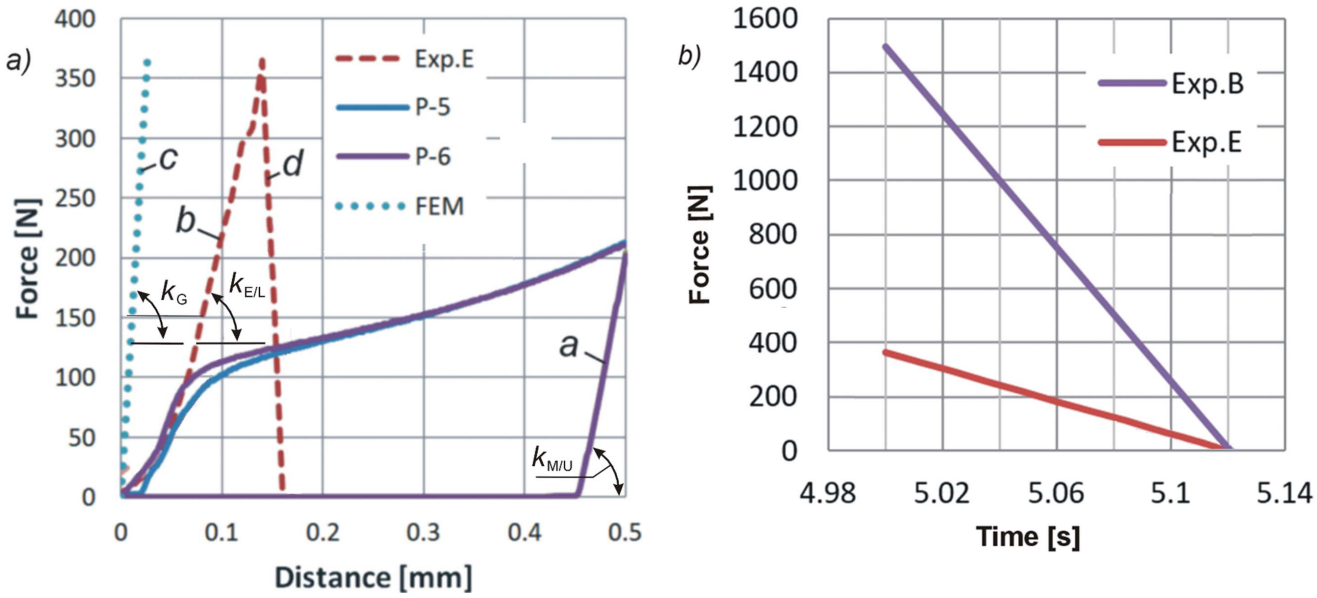

Fig. 8. (a) Comparison of selected strength records as a function of displacement: Exp. C, E and FEM – glass breaking by bending, P-5.6 – micro-upsetting, (b) selected results of force drop after fracture of glass samples in function of time

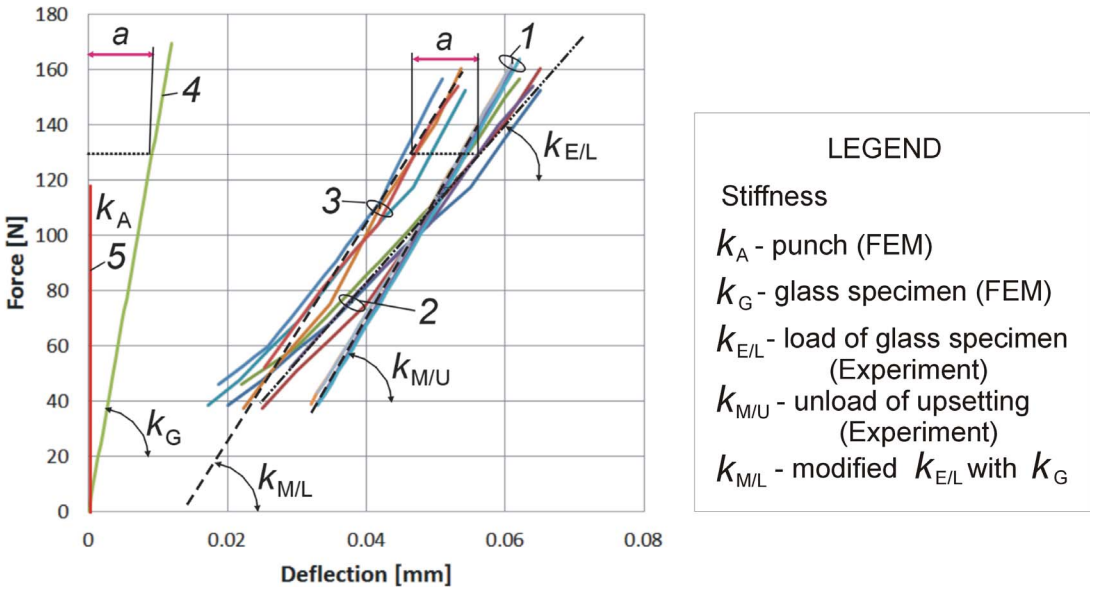

Fig. 9. Static analysis of the load system: 1 – set of curves of unloading in case of upsetting, 2 – set of load curves as a result of breaking the glass, 3 – set of curves from set 2 corrected by curve 4, 5 – deflection of the punch in FEM-1

The set of curves 1 contains the unloading curves in upsetting processes. The curve *a* in Fig. 8a corresponds to them. They are determined by stiffness $k_{M/U}$ (machine-unloading). The group 2 of curves contains the load curves in the glass breaking process. It corresponds to the curve *b* in Fig. 8a and is determined by the stiffness $k_{E/L}$. The stiffness of $k_{E/L}$ is influenced by the deflection of the glass sample before it is broken, determined by the stiffness k_G (Glass). This influence was determined on the basis of FEM simulation – line 4. The stiffness of the punch in FEM-model k_A – line 5 also affects the result of k_G, but the impact is so small that it is even difficult to see it in Fig. 9. The bending of the glass sample was included in the modification of the curves 2 to the corrected position 3. Each curve point has been offset parallel to the deflection axis by the correction resulting from the curve 4, see section *a* in Fig. 9. The corrected stiffness is now $k_{M/L}$, which is equal to $k_{M/U}$, which confirms the correctness of the analysis and measurements. This is the static stiffness of the load system, Table 2 – row 8.

7. Summary and Conclusions

- The use of ultrasonic vibrations at a frequency of 20 kHz and an amplitude of 16 μm and 5.8 μm in the micro-upsetting process of the cylindrical aluminium sample of a height and diameter of 1 mm causes a concentration of strain on both ends of the sample. There was observed (in relation to deformations of the sample without vibrations) 30-70% increase of cross-section area at ends of sample and a 20% decrease in cross-section area in the centre of the sample for 16 μm amplitude and 8-20% increase and 10% decrease respectively for 5.8 μm amplitude.
- The impact of vibrations covers, in the case of vibrations with an amplitude of 16 μm, approximately 27% and 20% of the length of the sample from the upper and lower surface respectively. In the case of vibrations with an amplitude of 5.8 μm, this influence covers about 10% of the sample height from both ends.
- Analyzing the course of forces of the upsetting process in the loading and unloading phase as well as the process of breaking glass samples, the spring deflections of key system elements and their natural frequencies were determined or calculated:
  - micro-sample
    A = 1.4 μm (punch vibrations amplitude 16μm) and
    A = 1.2 μm (punch vibrations amplitude 5.8 μm),
    f = 22.8 MHz,
  - lower punch
    A = 1.89 μm (punch vibrations amplitude 16μm) and
    A =1.45 μm (punch vibration amplitude 5.8 μm),
    f = 0.530 MHz,
  - load system (all)
    A = 33/ 25 μm, respectively for punch vibration amplitude 16/5.8 μm,
    f about 20 Hz.

These estimated values shows that in case of 16 μm amplitude of vibration the security factor (16 / 3.24) is about 4.32, which indicates that during the upsetting process the face of the punch detaches from the surface of the sample. In the case of vibrations with amplitude of 5.8 μm, the security factor is (5.8 / 3.29) about 1.76, which in the case of a large approximation of calculations does not determine the loss of contact. From the comparison of the course of forces, it seems that the process with the use of lower amplitude oscillations proceeded at the limit of loss of contact.

- A possible effect of ultrasonic vibrations is the temperature rise during deformation at both ends of the sample. Such a hypothetical increase was estimated based on the deformation of the layers near the contact of the sample with tools. The hypothetical increase in temperature is 150-200°C for an amplitude of 16 μm and a maximum of 100°C for an amplitude of 5.8 μm.

Acknowledgements

The work presented in this paper is financially supported by the National Science Centre – Poland (UMO-2011/01/B/ST8/07731).

REFERENCES

[1] Y. Saotome, H. Iwazaki, J. of Mat. Proc. Tech. **119** (1-3), 307-311 (2001).
[2] M. Geiger, U. Engel, Prod. Eng. **II**, 15-18 (1994) .
[3] M. Jiang, G. Feng, Z. Yang, W. Zeng, Int. J. Adv. Manu. Technol. **82**, 1363-1369 (2016).
[4] M. Geiger, M. Kleiner, R. Eckstein, N. Tiesler, CIRP Annals – Manufac. Techn. **50** (2), 445-462 (2001).
[5] A. Kocańda, W. Presz, G. Adamczyk, P. Czyżewski, J. of Mat. Proc. Tech. **60** (1-4), 23-30 (1996).
[6] N. Tiesler, Wire **52** (1), 34-38 (2002) .
[7] U. Engel, Wear **260** (3), 265-273 (2006).
[8] C. Wang, B. Guo, D. Shan, M. Zang, X. Bai, Int. J. Adv. Manuf. Technol. **71** (9-12), 2083-2090 (2014).
[9] W. Presz, The Method of determining the tendency to galling in vibration assisted microforming, in Metal, 27th Int. Conf. on Metallurgy and Materials **63**, 450-456 (2018)
[10] A. Muster, W. Presz, Scandinavian J. of Metallurgy **28** (1) 5-8 (1999).
[11] T. Salacinski, T. Chmlelewski, M. Winiarski, Adv. in Mat. Science **18** (1) 20-27 (2018).
[12] W. Presz, R. Cacko, Determination of material distribution in heading process of small bimetallic bar, in AIP Conf. Proc. **1960** (1**)**, 050014 (2018).
[13] E. Ghassemali, M.J. Chan, C.B. Wah, A.E. W. Jarfors, S.C.V. Lin, Mat. Science and Eng. **582**, 379-388 (2013).
[14] L. Olejnik, W. Presz, A. Rosochowski, Int. J. of Mat. Form. **2** (1), 617-620 (2009).

[15] J.Q. Ran, M.W. Fu, W.L. Chan, Int. J. of Plasticity **41**, 65-81 (2013).
[16] W. Presz, B. Andersen, T. Wanheim, J. of Achiev. in Mat. and Manuf. Eng. **18** (1-2) 411-414 (2006).
[17] E. Cannella, E.K. Nielsen, A. Stolfi, Micromachines **8** (7), 214-230 (2017).
[18] N.A. Paldan, M. Arentoft, R.S. Eriksen, C. Mangeot, Int. J. Mater. Form, **1** (1), 467-470 (2008)
[19] W. Presz, Com. Methods in Mat. Science **16**, 196-203 (2016).
[20] W. Presz, M. Rosochowski, Procedia Eng. **207**, 1004-1009 (2017).
[21] E. Ghassemali, A.E. Jarfors, M.-J. Tan, S.C.V. Lin, Int. J. of Mat. Form **6**, 65-74 (2013).
[22] T. Stellin, R. Tiium, U. Engel, Prod. Eng. **10**, 103-112 (2016).
[23] G.E. Nevill, F.R. Brotzen, ASTM Proc. **57**, 751-758 (1957).
[24] F. Blaha, B. Langenecker, Acta Metallurgica **7** (2), 93-100 (1959).
[25] F. Djavanrood, H. Ahmadian, K. Koohkan, R. Naseri, Ultrasonics **53** (6), 1086-1096 (2013).
[26] B. Christina, N. Gracious, Ultrasonics **51** (5), 606-616 (2011).
[27] J.-C. Hung, C. Hung, Ultrasonics **43** (8), 692-698 (2005).
[28] S.A. Aziz, M. Lucas, App. Mech. and Mat. **24-25**, 311-316 (2010).
[29] W. Presz, R. Cacko, Ultrasonic assisted microforming, in: Metal, 26th Int. Conf. on Metallurgy and Materials 521-526 (2017).
[30] T. Shimizu, T. Kakegawa, M. Yang, Proc. Eng. **81**, 1884-1889 (2014).
[31] Y. Daud, M. Lucas, Z. Huang, Ultrasonics, 44 (sup.), 511-515 (2006).
[32] H. Zhou, H. Cui, Q.-H. Qin, H. Wang, Mat. Science and Eng. **682**, 376-388 (2017).
[33] J. Hu, T. Shimizu, T. Yoshino, T. Shiratori, M. Yang, J. of Mat. Proc. Tech. **258**, 144-154 (2018).
[34] W. Presz, Dynamic effect in ultrasonic assisted micro-upsetting, in: AIP Conf. Proc. **1960** (1). 100012 (2018).
[35] J.C. Hung, Y.C. Tsai, Mat. Scie. and Eng. **580**, 125-132 (2013).
[36] R. Raja, S. Lakhinaraihan, P. Murugesan, Int. J. of Modern Eng. Reserch **3** (6), 3852-3862 (2013).
[37] Z. Yaoa, G.-Y. Kim, L. Fadley, Q. Zou, D. Mei, Z. Chen, J. of Mat. Proc. Tech. **212** (3), 640-646 (2012).
[38] Y. Liu, S. Suslow, O. Han, L. Hua, X. Clause, Met. and Mat. Trans. **44**, 3232-3244 (2013).
[39] J. Hu, T. Shimizu, M. Yang, Ultr. Sonochem. **48**, 240-248 (2018).
[40] W. Presz, The Method of Micro-Upsetting in Uneven Temperature Distribution, in: METAL, 27th Int. Conf. on Metallurgy and Mat. 323-329 (2018).
[41] Atlas of Stress-Strain Curves, Second Edition, Materials Park, OH 44073-0002.